Additive manufacturing of patterned 2D semiconductor through recyclable masked growth

Yunfan Guo[a], Pin-Chun Shen[a], Cong Su[b], Ang-Yu Lu[a], Marek Hempel[a], Yimo Han[c], Qingqing Ji[a], Yuxuan Lin[a], Enzheng Shi[d], Elaine McVay[a], Letian Dou[d], David A. Muller[c], Tomás Palacios[a], Ju Li[b], Xi Ling[e,f,g,1], and Jing Kong[a,1]

[a]Department of Electrical Engineering and Computer Science, Massachusetts Institute of Technology, Cambridge, MA 02139; [b]Department of Nuclear and Materials Science and Engineering, Massachusetts Institute of Technology, Cambridge, MA 02139; [c]School of Applied & Engineering Physics, Cornell University, Ithaca, NY 14850; [d]Davidson School of Chemical Engineering, Purdue University, West Lafayette, IN 47907; [e]Department of Chemistry, Boston University, Boston, MA 02215; [f]Division of Materials Science and Engineering, Boston University, Boston, MA 02215; and [g]The Photonics Center, Boston University, Boston, MA 02215

Edited by Ramamoorthy Ramesh, University of California, Berkeley, CA, and accepted by Editorial Board Member Zachary Fisk January 12, 2019 (received for review September 18, 2018)

The 2D van der Waals crystals have shown great promise as potential future electronic materials due to their atomically thin and smooth nature, highly tailorable electronic structure, and mass production compatibility through chemical synthesis. Electronic devices, such as field effect transistors (FETs), from these materials require patterning and fabrication into desired structures. Specifically, the scale up and future development of "2D"-based electronics will inevitably require large numbers of fabrication steps in the patterning of 2D semiconductors, such as transition metal dichalcogenides (TMDs). This is currently carried out via multiple steps of lithography, etching, and transfer. As 2D devices become more complex (e.g., numerous 2D materials, more layers, specific shapes, etc.), the patterning steps can become economically costly and time consuming. Here, we developed a method to directly synthesize a 2D semiconductor, monolayer molybdenum disulfide (MoS_2), in arbitrary patterns on insulating SiO_2/Si via seed-promoted chemical vapor deposition (CVD) and substrate engineering. This method shows the potential of using the prepatterned substrates as a master template for the repeated growth of monolayer MoS_2 patterns. Our technique currently produces arbitrary monolayer MoS_2 patterns at a spatial resolution of 2 μm with excellent homogeneity and transistor performance (room temperature electron mobility of 30 $cm^2\ V^{-1}\ s^{-1}$ and on–off current ratio of 10^7). Extending this patterning method to other 2D materials can provide a facile method for the repeatable direct synthesis of 2D materials for future electronics and optoelectronics.

2D semiconductor | monolayer MoS_2 | patterned growth | growth mechanism | recyclable masked growth

In recent years, the family of monolayer transition metal dichalcogenides (TMDs) has become attractive semiconducting crystals for nano- and flexible electronics due to their atomic thinness, high carrier mobility, and excellent flexibility (1, 2). In addition, TMDs have drawn considerable attention in condensed matter due to the unique electronic band structures and intriguing valley–spin coupling, making them promising for valleytronics (3), piezoelectrics (4), bandgap modulation (5), and high-quantum efficiency optical/optoelectronic applications (6, 7).

To fabricate future 2D-based electronics and optoelectronics structures, it is necessary to pattern 2D materials for contacts, gating, optical access, etc. (8, 9). At present, patterning TMDs have relied on either subtractive or additive manufacturing. "Growth and etch" (10–12) is perhaps the most typical method of 2D patterning, where it utilizes subtractive manufacturing (akin to "top down") to lithographically define and subsequently etch away unwanted areas of 2D material. This method has spatial resolution roughly down to nanometers (when using electron beam lithography), but it has a high manufacturing cost and can become time consuming. Additionally, the inevitable generation of multiple layers (which is necessary when constructing an integrated system) becomes difficult to handle, as selective etching of 2D materials still poses fabrication challenge (also due to their atomic thinness). Furthermore, contaminations between interfaces and rough, amorphous edge terminations may be introduced during fabrication, thus increasing the chance for quality deterioration of as-grown materials. To avoid surface contamination by resist residues, shadow mask (13) and laser cutting (14) can be considered, but the poor spatial resolutions typically are in the range of near millimeters to hundreds of micrometers.

However, for additive manufacturing ("bottom-up") techniques, inkjet printing (15) has been extensively used for the large-scale preparation of TMD patterns. Nevertheless, it requires solution-based 2D flakes (typically multilayered), and the minimal feature size is usually larger than 10 μm. Various efforts have been devoted to prepattern seed precursors [molybdenum oxide (MoO_3), ammonium heptamolybdate (16), or Au catalyst (17)] to generate patterned TMD structures directly, although preventing multilayer islands growing on monolayer regions still turned out to be challenging. Substrate modification by O_2 plasma provides a simpler route to patterned TMDs (18, 19), but the reported electrical mobility has been two orders of magnitude lower than as-grown TMDs ($1\ cm^2\ V^{-1}\ s^{-1}$) with poor spatial resolution (~100 μm).

Significance

Traditional semiconductor fabrication methods, such as lithography and etching, have been sufficient for the needs of integrated circuits over past decades. Their applicability has also been demonstrated in emerging 2D materials, which offers facile processing over large lateral dimensions, while unique and remarkable properties due to the confinement within atomic thicknesses. Nevertheless, each fabrication step adds cost to the manufacturing and increases the possibility of quality degradation. Here, we developed a method to directly synthesize arbitrary monolayer molybdenum disulfide patterns with high spatial resolution, excellent homogeneity, and electrical performance on insulating SiO_2/Si. Significantly, our on-demand method allows for the repeated growth of patterned 2D materials with preserved structural integrity and material qualities, paving the way for simpler and cost-effective fabrication.

Author contributions: Y.G. and J.K. designed research; Y.G., P.-C.S., C.S., A.-Y.L., M.H., Y.H., and E.M. performed research; Y.G., P.-C.S., C.S., Q.J., Y.L., E.S., L.D., D.A.M., T.P., J.L., X.L., and J.K. analyzed data; and Y.G., P.-C.S., C.S., and J.K. wrote the paper.

The authors declare no conflict of interest.

This article is a PNAS Direct Submission. R.R. is a guest editor invited by the Editorial Board.

[1]To whom correspondence may be addressed. Email: xiling@bu.edu or jingkong@mit.edu.

This article contains supporting information online at www.pnas.org/lookup/suppl/doi:10.1073/pnas.1816197116/-/DCSupplemental.

Published online February 12, 2019.

ENGINEERING

Herein, through in-depth studies of the growth mechanism and precursor control, we have found that plasma-based substrate modification can be used to directly grow patterned monolayer molybdenum disulfide (MoS_2) with high crystal quality, diverse geometries, high spatial resolution (2 μm at present, limited by laser lithography), and high electrical mobility (~30 cm^2 V^{-1} s^{-1}) on SiO_2/Si substrate. The same patterning mask can be recycled for repeated growth with consistent material morphology and quality each time, which demonstrates the potential of this method for a "master–replica" type of repeated manufacturing. Such an additive manufacturing method opens up the possibilities for wide applications of 2D TMD nanostructures in modern electronics and optoelectronics with much simpler fabrication.

Results and Discussions

Substrate modification is the first step to achieve the patterned MoS_2 structures as shown in Fig. 1*A*. As a proof of concept, we have chosen to define MoS_2 in the shape of kirigami patterns. Traditionally, kirigami is a technique to create 3D structures from 2D sheets and has been applied in 2D materials to build robust macro- or microscale structures with tunable mechanical properties (20–22). Photolithography defines patterns of photoresist on the substrates (*SI Appendix*, Fig. S1) while undeveloped areas are etched away using O_2 plasma, which simultaneously modifies the surface of SiO_2 substrate. After removing the developed photoresist, MoS_2 can selectively grow on plasma-treated areas, similar to our previous studies (details are in *Methods*) (23, 24). As the plasma treatment creates a region with higher surface energy and enhanced hydrophilicity (discussion below), the hydrophilic salt perylene-3,4,9,10-tetracarboxylic acid tetrapotassium (PTAS) is used to promote seeded, selective MoS_2 growth only at the O_2 plasma-treated areas, forming as-grown patterned MoS_2.

Inspection of the resultant growth using optical microscopy (OM) clearly shows a patterned growth of MoS_2 (in the shape of a wave array) on SiO_2/Si (Fig. 1*B*). The reflectance contrast of the green-tinted MoS_2, which comprises the wave, is uniform, with a strap width of 20 μm (tunable by changing the patterns on the substrate). Fig. 1*C* shows that MoS_2 grows at opposite locations (in contrast to Fig. 1*B*) when a negative photoresist was used for the same pattern. Through this technique, monolayer MoS_2 patterns with diverse morphologies and different feature sizes can be obtained by only changing the original growth "mask" (*SI Appendix*, Fig. S2 *A1–C2*). Currently, the minimal spatial resolution is 2 μm, which is limited by the direct laser writing instrument (*SI Appendix*, Fig. S2 *D1* and *D2*). To evaluate the surface morphology of the MoS_2 patterns, we use atomic force microscopy (AFM). We first observed that the strong O_2 plasma etching causes a height difference between the pristine SiO_2 regions and the etched regions of about 2 nm (*SI Appendix*, Fig. S3*A*). After the growth of MoS_2, a flat and pristine monolayer fills in the recessed region (Fig. 1*D*) and reduces the height difference to ~1.3 nm (*SI Appendix*, Fig. S3*B*), confirming that the thickness of MoS_2 patterns is monolayer (~0.7 nm).

To evaluate the crystallinity of the monolayer MoS_2 patterns, characterizations with photoluminescence (PL) and Raman spectroscopy were carried out. A strong PL emission at around 1.85 eV with an FWHM intensity of about 60 meV was observed on all tested samples, consistent with the emission of grown monolayer MoS_2 (Fig. 1*G*) (25). For Raman spectroscopy, the frequency difference between Raman peaks located at 383 cm^{-1}

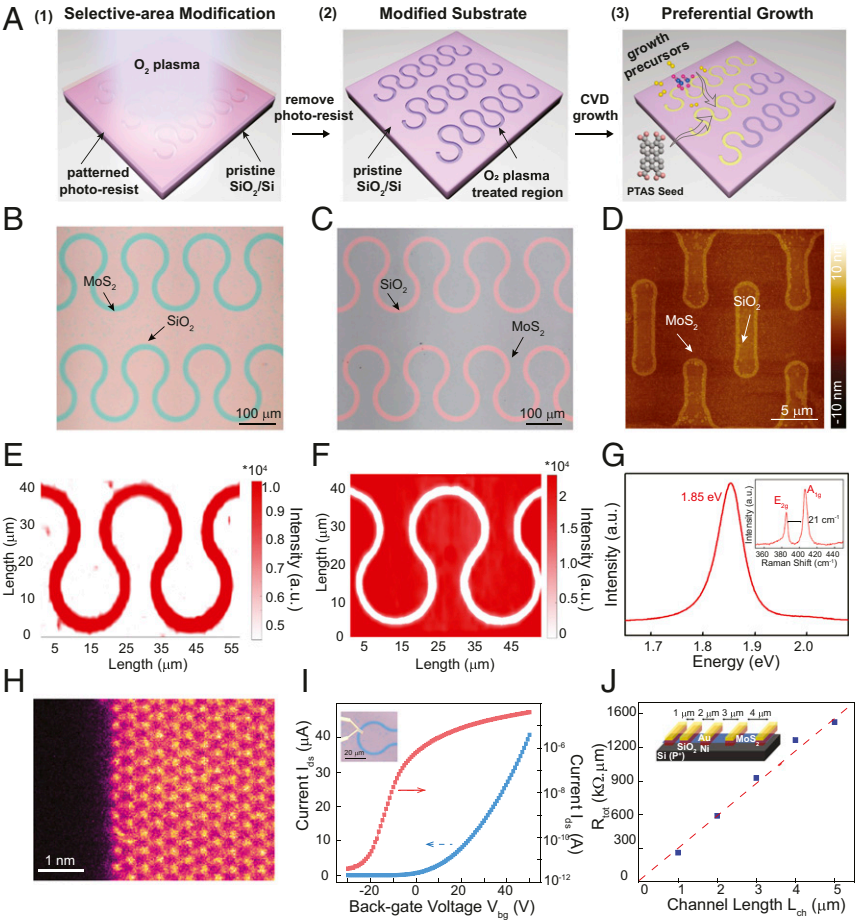

Fig. 1. Patterned growth and characterization of MoS_2 nanostructures. (*A*) Schematic representation of the procedures for the direct growth of MoS_2 nanostructures via seed-promoted growth and substrate engineering. Step 1: the selective-area modification process by lithography patterning and O_2 plasma etching; step 2: the patterned regions are distinguished from pristine SiO_2/Si substrates after modification; step 3: the preferential growth of MoS_2 on patterned SiO_2/Si regions. (*B*) A typical OM image of a monolayer MoS_2 wave array. (*C*) OM image of a monolayer MoS_2 wave film that grows at the opposite locations when a negative photoresist was used for the wave pattern in *B*. (*D*) AFM image of a monolayer MoS_2 kirigami structure showing the flat surface and ordered edge morphology. (*E* and *F*) PL mappings for monolayer MoS_2 wave arrays and the inversed wave film pattern. (*G*) A typical PL spectrum collected on the monolayer MoS_2 wave structures. (*Inset*) A typical Raman spectrum collected on the monolayer MoS_2 wave structures. (*H*) ADF-STEM image of a patterned monolayer MoS_2 edge showing the clean and ordered edge at atomic scale. (*I*) Transfer ($I_{ds} - V_{bg}$) characteristic of a typical back-gated transistor fabricated on our CVD-patterned MoS_2 film with gate voltages from −30 to 50 V and a bias V_{ds} fixed at 1 V. The room temperature electron mobility of the transistor is 29.3 cm^2 V^{-1} s^{-1}. The red curve shows the transfer characteristic of the same MoS_2 transistor in logarithmic scale. The on–off current ratio is ~10^7. (*Inset*) Optical image of a typical MoS_2 device based on the wave pattern. (*J*) Total device resistance R_{TOT} normalized by width vs. channel length L_{ch} measured at a carrier concentration n of ~ 1.8 × 10^{12} cm^{-2}, yielding a contact resistance of R_c ~ 6.7 kΩ.μm from the vertical intercept. (*Inset*) The schematic of our TLM devices with Ni/Au contacts.

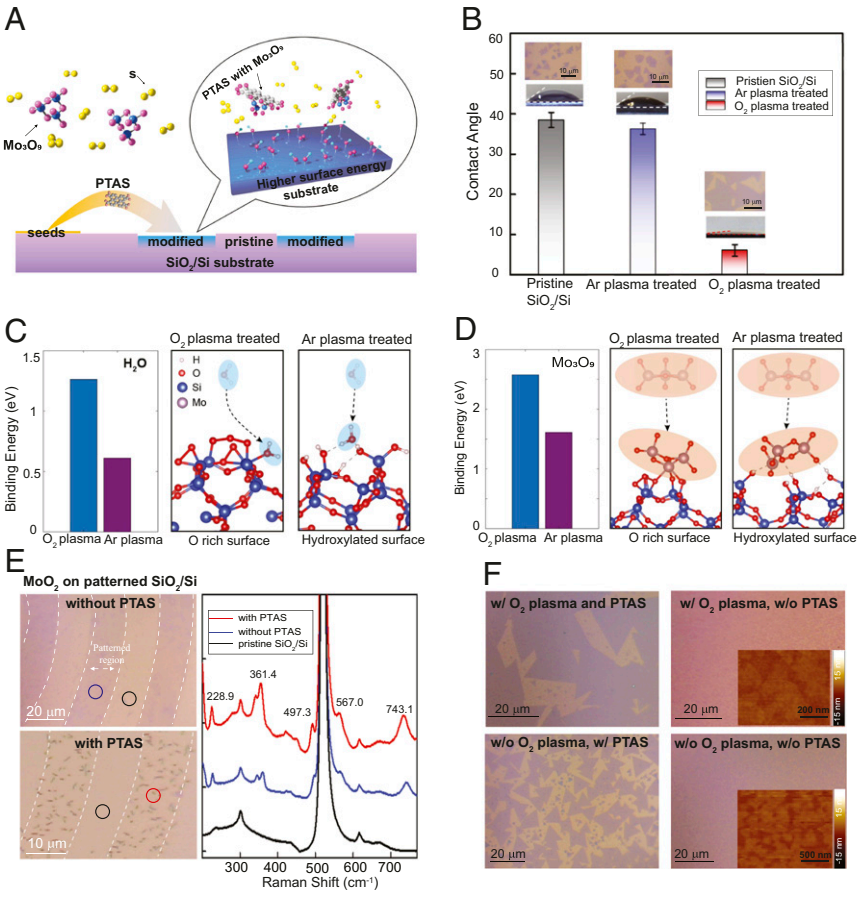

Fig. 2. Mechanism study for the patterned growth of monolayer MoS_2 nanostructures. (*A*) Schematic illustration of the growth mechanism of the patterned growth of MoS_2. (*B*) Comparison of contact angles for pristine, Ar plasma-treated, and O_2 plasma-treated SiO_2/Si substrates. (*C*) DFT calculation for the binding energies between H_2O and SiO_2/Si substrate treated by O_2 plasma and Ar plasma. (*D*) DFT calculation for the binding energies between Mo_3O_9 and SiO_2/Si substrate treated by O_2 plasma and Ar plasma. (*E*, *Upper Left*) OM image of MoO_2 particles preferentially deposited on patterned SiO_2/Si regions without PTAS. (*E*, *Lower Left*) OM image of MoO_2 particles preferentially deposited on patterned SiO_2/Si regions with the presence of PTAS. (*E*, *Right*) Raman spectra collected at the regions indicted by the red, blue, and black circles in the OM images in *Left*; several MoO_2 Raman peaks are labeled in the spectra. It is shown that MoO_2 particles exhibit a clear preference to deposit on the patterned region and that the Raman peaks of MoO_2 are stronger with the presence of PTAS. (*F*, *Upper Left*) OM image of monolayer MoS_2 flakes grown on O_2 plasma-treated SiO_2/Si substrate with the assistance of PTAS. The domain size of MoS_2 is around 20 μm. (*F*, *Upper Right*) OM image of small MoS_2 flakes grown on O_2 plasma-treated SiO_2/Si substrate without PTAS. (*Inset*) AFM images of MoS_2 small flakes with domain size around 300 nm. (*F*, *Lower Left*) OM image of monolayer MoS_2 flakes grown on pristine SiO_2/Si substrate with the assistance of PTAS. The domain size of MoS_2 is around 8–10 μm. (*F*, *Lower Right*) OM image of small MoS_2 flakes grown on pristine SiO_2/Si substrate without PTAS seed. (*Inset*) AFM images of MoS_2 small flakes with domain size around 200 nm, indicating the poor quality of MoS_2 growth.

(E_{2g}) and 404 cm^{-1} (A_{1g}) is 21 cm^{-1}, further confirming that the patterned MoS_2 is monolayers as well (Fig. 1*G*, *Inset*). To assess the spatial homogeneity, we performed PL and Raman mappings across the grown structures. PL mappings at 670 nm in Fig. 1 *E* and *F* and *SI Appendix*, Fig. S4 *C2* and *D2* confirmed that monolayer MoS_2 follows the prepared wave and rectangle kirigami patterns reasonably well with crystalline homogeneity. Additionally, Raman mappings of the E_{2g} mode (*SI Appendix*, Fig. S4 *A2*, *B2*, *C3*, and *D3*) and the A_{1g} mode (*SI Appendix*, Fig. S4 *A3*, *B3*, *C4*, and *D4*) both exhibit a high degree of spatial uniformity. All optical spectroscopy data indicate that this patterned manufacture produces high-quality MoS_2.

Through transmission electron microscopy (TEM) examination, it was found that the patterned MoS_2 maintains reasonably sharp and clean edges. *SI Appendix*, Fig. S5*A* shows a typical bright-field TEM image of an MoS_2 edge, while *SI Appendix*, Fig. S5*B* shows the corresponding dark-field TEM and diffraction pattern (*SI Appendix*, Fig. S5*B*, *Inset*). Through the dark-field TEM, the patterned MoS_2 can be clearly observed as polycrystalline (typical in all of these growth results) with three domains. Excluding a wrinkle likely caused by the TEM transfer process, there is no visible gap or bilayer area over the film. Particularly, the edges formed by domain merging remain flat and sharp. Compared with the growth-and-etch method, one additional advantage for this direct growth is that the as-grown edges are clean, are sharp, and exhibit fewer contaminations or atomic defects as revealed by the atomic-resolution annular dark-field scanning TEM (ADF-TEM) image (shown in Fig. 1*H*). This is imperative in preserving the intrinsic properties of TMD materials, especially for electrical performance.

In conventional nanofabrication or device manufacturing, photolithography and subsequent plasma etching are necessary to define individual devices from the continuous film, which can degrade the performance of the devices, as photoresist residues may induce scattering centers and high contact resistances at the interface. In comparison, patterned monolayer MoS_2 at predefined positions would preserve intrinsic electronic properties and facilitate the system-level fabrication for multifunctional devices (Fig. 1*I*, *Inset*). To evaluate the electronic performance, we fabricated back-gated field effect transistors (FETs) on different monolayer MoS_2 patterns. Our MoS_2 FETs shows high performance based on the average electronic properties (*SI Appendix*, Fig. S6). Fig. 1*I* and *SI Appendix*, Fig. S7*A* exhibit the typical transfer ($I_{ds} - V_{bg}$) and output ($I_{ds} - V_{ds}$) characteristics, respectively, of an FET fabricated on an MoS_2 wave pattern. The MoS_2 transistor exhibits *n*-type conduction with I_{on}/I_{off} ratio up to ~10^7. The electron mobility of our MoS_2 FET reaches 29.3 cm^2 V^{-1} s^{-1} at room temperature in air (Fig. 1*I*), which is comparable with the reported values of metal–organic chemical vapor deposition-grown samples (26). Furthermore, the contact resistance (R_c) of our MoS_2 FETs was further extracted based on the transfer length method (TLM). Fig. 1*J* shows a linear fit to the total resistance normalized by channel width (R_{TOT}) vs. channel length (L_{ch}). We extract $R_c \sim 6.7$ kΩ·μm at room temperature for a carrier density *n* of about 1.8×10^{12} cm^{-2}. This contact resistance is consistent with previous reported values of Ni-contacted MoS_2 devices on exfoliated samples (27). Significantly, one of the crucial factors to achieve a low contact resistance is the clean interface between MoS_2 and metal electrodes, which is attained through the direct growth of MoS_2 patterns.

Understanding the growth mechanism is critical to obtaining reliable predefined MoS_2 patterns via such direct growth paradigm. To this end, we systematically investigated the substrate modification, seed-promoted nucleation, and the effect of the sulfur vapor on the growth process. A generic mechanism of thin film growth considers chemical potentials and surface energies of

epitaxial layers and the substrates (28). Therefore, increasing the surface energy on selective areas of the substrate favors patterned monolayer growth over the growth of multilayer particles. As shown in Fig. 2*A*, after patterning and O_2 plasma treatment, the SiO_2/Si substrate was composed of modified regions and pristine regions. We compared the contact angles for each type of surface in Fig. 2*B*. The contact angle of pristine SiO_2/Si substrate is around 38.48°, while it drops rapidly to 6.04° after O_2 plasma treating for 10 min, similar to observations in previous reports (19). To compare the change in the physical surface due to O_2 plasma treatment, we also measured the contact angle of the surface treated by Ar plasma for the same duration (which gives similar surface roughness) (*SI Appendix*, Fig. S8). However, the Ar plasma-treated substrate shows a contact angle of about 36.22°, similar to that of the pristine SiO_2/Si. Thus, physical roughness is not the main contribution to the surface energy change.

To understand the difference in surface energies induced by different treatments, we conducted density functional theory (DFT) calculations. In our model, Ar plasma etching increases the number of dangling bonds on the surface of SiO_2/Si substrate, which serve as active sites to dissociate H_2O molecules in ambient environment, resulting in a hydroxylated surface (terminated by –OH group) (*SI Appendix*, Fig. S9). However, in the case of O_2 plasma, the oxygen bonds on the unsaturated surface site and yields an oxygen-rich surface. DFT calculations show that the binding energy of water with the oxygen-rich surface is over two times that of the Ar plasma-treated surface (Fig. 2*C*), consistent with the contact angle measurement in Fig. 2*B*. When considering the binding energy with Mo_3O_9 [the intermediate of MoO_{3-x} during the MoS_2 growth (29)], the oxygen-rich surface has ∼1-eV higher binding energy than that of the hydroxylated surface (Fig. 2*D*). Combining the growth result (*SI Appendix*, Fig. S10) with DFT calculations, it is shown that the O_2 plasma-modified substrates have better wettability and higher binding energy to Mo_3O_9, which is beneficial for the monolayer growth of MoS_2. We experimentally verify this via results shown in Fig. 2*E*. On only supplying MoO_3 powder during the growth, Mo-containing species [MoO_2 as confirmed by Raman spectroscopy (30)] clearly preferred the O_2 plasma-treated regions over the nontreated regions. By adding PTAS, which is a hydrophilic salt and has preference for the patterned regions (23), Mo-based compounds may have higher adsorption within the patterned regions (as given by a stronger Raman signature after PTAS was added). Here, the presence of PTAS may increase the strength of surface adhesion between MoS_2 and SiO_2/Si, leading to the monolayer growth of MoS_2. Based on the different growth results in Fig. 2*F*, which show obvious growth enhancement under O_2 plasma and PTAS, we conclude that the combination of O_2 plasma treatment and PTAS exhibits a synergetic effect that promotes the optimized MoS_2 growth.

For the MoS_2 growth to distinguish the difference between the untreated and treated surfaces, we noted that the entrance timing of sulfur and its amount are critical, both of which will affect the concentration (or partial pressure) of sulfur in the gaseous phase. According to the Mo–O–S phase diagram (31), MoO_3 undergoes a two-step reaction in the chemical vapor deposition (CVD) growth of MoS_2 (32):

$$MoO_3(s) + x/2S(g) \rightarrow MoO_{3-x}(g) + x/2SO_2(g). \quad [1]$$

Next, $MoO_{3-x}(g)$ has two possible reaction paths:

$$MoO_{3-x}(g) + (7-x)/2S(g) \rightarrow MoS_2(s) + (3-x)/2SO_2(g) \quad [2.1]$$

$$MoO_{3-x}(g) + (1-x)/2S(g) \rightarrow MoO_2(s) + (1-x)/2SO_2(g). \quad [2.2]$$

Higher [S]/[Mo] ratio (here, [S] and [Mo] indicate the concentrations or partial pressures of S and Mo species) promotes the reaction in path [**2.1**], while lower [S]/[Mo] ratio tends to form MoO_2 as path [**2.2**]. To investigate the role of sulfur, we laid several patterned substrates as shown in *SI Appendix*, Fig. S11*A* (23). Presumably, the sulfur concentration decreases along the substrate as the distance away from the sulfur source increases, and the quality of the MoS_2 patterns in different regions of SiO_2/Si reflects the influence of sulfur concentration on the patterned growth. Instead of producing spatially distinguished MoS_2 patterns, higher sulfur concentration creates a continuous MoS_2 film across the entire surface (*SI Appendix*, Fig. S11*B*) (which means that there is no selective patterning by the substrate), while lower sulfur concentration produces discontinuous MoS_2 flakes (*SI Appendix*, Fig. S11*E*). Only under an appropriate concentration, we can produce patterned monolayer MoS_2 (*SI Appendix*, Fig. S11*D*). Therefore, we designed an improved CVD setup to control sulfur concentration during the growth. As shown in Fig. 3*A*, a small quartz tube is used to carry the sulfur boat, and a set of magnets is used to move the position of the sulfur boat. The sulfur powder is initially kept outside of the heating zone, and it is moved inside the heating zone during the ramping period when the MoO_3 precursor reaches a suitable temperature (*SI Appendix*, Fig. S12) (it takes 15 min for the center of the furnace to reach the growth temperature). We first found that the entrance timing of sulfur impacts the ratio of sulfur partial pressure to Mo partial pressure ([S]/[Mo]) due to the temperature difference at different entrance times (*SI Appendix*, Fig. S13 and Table S1). As shown in Fig. 3*B*, the [S]/[Mo] ratio has a negative correlation with the entrance timing of

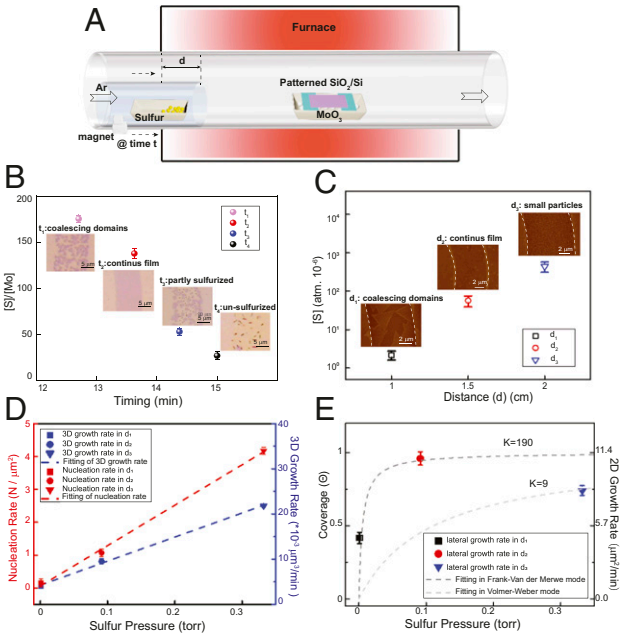

Fig. 3. The control of sulfur precursor during the patterned growth of monolayer MoS_2 nanostructures. (*A*) Schematic illustration of the modified CVD setup and the controlled process to synthesize patterned MoS_2 nanostructures. (*B*) The relationship between the entrance time of the sulfur precursor and the corresponding [S]/[Mo] ratio during the growth. (*Insets*) OM images of different growth results according to different entrance times of sulfur. (*C*) The relationship between the locations of the sulfur precursor (d) and the corresponding vapor pressures of sulfur. (*Insets*) AFM images of MoS_2 patterns grown as a result of different precursor locations. (*D*) The dependence of nucleation rate as the function of partial pressure of sulfur precursor (left *y* axis); the dependence of 3D growth rate as the function of partial pressure of sulfur precursor (right *y* axis). (*E*) The dependence of surface coverage as the function of partial pressure of sulfur precursor (left *y* axis); the dependence of 2D growth rate as the function of partial pressure of the sulfur precursor (right *y* axis).

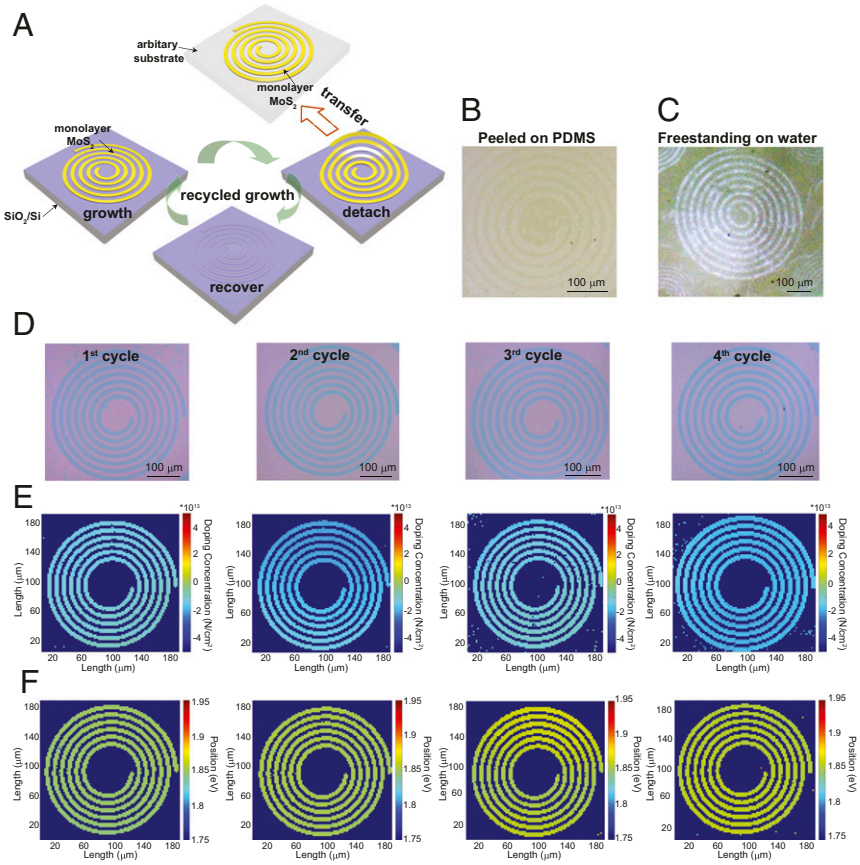

Fig. 4. Repeated growth of patterned monolayer MoS_2 nanostructures using the same template. (*A*) Schematic illustration of repeated growth procedures for directly grown MoS_2 patterns. (*B*) OM image of monolayer MoS_2 patterns peeled on PDMS. (*C*) OM image of monolayer MoS_2 structures freestanding on water without any additional support. (*D*) OM images of the monolayer MoS_2 spiral pattern after the first, second, third, and fourth growth cycles. (*E*) The carrier concentration mappings (via Raman) of the monolayer MoS_2 spiral after the first, second, third, and fourth growth cycles as given by *D*. (*F*) The photoluminescence position mappings (via PL spectrum) of the monolayer MoS_2 spiral after the first, second, third, and fourth growth cycles as given by *D*.

sulfur, which essentially dominates the degree of the sulfurization in the process. When sulfur is introduced relatively early (as shown in Fig. 3*B*) (at t_1 or t_2; before 14 min), the [S]/[Mo] is high enough to fully sulfurize MoO_3 into MoS_2. Nevertheless, to make continuous MoS_2 patterns, sufficient supply of molybdenum is also required (entering at t_2) compared with the lower supply of molybdenum at t_1. However, when sulfur enters at t_3, the [S]/[Mo] ratio decreases rapidly, resulting in only a part of MoO_3 turning into MoS_2. If sulfur enters at t_4 or later, only black MoO_2 particles are obtained on the substrate. Although MoO_2 can also be sulfurized into MoS_2 (33), the temperature needed (650 °C to 850 °C) is much higher than that in our growth. Additionally, the position where the sulfur boat is introduced (corresponding to the distance d in Fig. 3*C* and as illustrated in Fig. 3*A*) is another important factor of sulfur pressure, which therefore, determines the nucleation rate and growth rate of MoS_2. According to the temperature variation at different positions (i.e., different d values) (*SI Appendix*, Fig. S14), we semiquantitatively calculated the nucleation rate and the growth rate of the patterned growth of monolayer MoS_2 (*SI Appendix*, Table S2). In Fig. 3*C*, the [S] at d_1 is insufficient, leading to both low nucleation rate (Fig. 3*D*) and growth rate (Fig. 3*E*). While excess [S] at d_3 will increase the nucleation rate of MoS_2 dramatically, it also accelerates the MoS_2 nuclei growth rate in the vertical direction (corresponding to the 3D growth rate in Fig. 3*D*), which is significantly faster than that in the lateral direction (corresponding to 2D growth rate in Fig. 3*E*), leading to the formation of multilayer MoS_2 particles. If the sulfur partial pressure is kept at an appropriate value (located at d_2), we could achieve medium nucleation rate and optimal growth rate in the lateral direction and obtain monolayer MoS_2 patterns.

As previously mentioned, electronic applications require patterned materials for device fabrication and integration. Nevertheless, previous methods to produce patterned 2D materials are limited by the single use of patterned substrates or etched materials. Therefore, developing a master–replica type of repeated growth of patterned TMD materials is highly attractive for 2D material device fabrication. Here, we have found that the prepatterned substrate can be repeatedly used through the noninvasive transfer of monolayer MoS_2 patterns. As shown in Fig. 4*A*, due to the weak interaction between the monolayer MoS_2 and the SiO_2/Si substrate, monolayer MoS_2 patterns can be easily detached (with preserved structural integrity) from the substrate by directly peeling with a polydimethylsiloxane (PDMS) stamp via dry transfer (Fig. 4*B*) or delaminating by water via wet transfer (Fig. 4*C* and *SI Appendix*, Figs. S15 and S16). Since the separation process is performed without any intermediate supporting layer or etchant, the released substrate with original patterns is recovered, which makes it possible for the next cycle of patterned growth. In our study, it was found that the patterned substrate can be reused at least four times without seeing signs of wear, and the quality of monolayer MoS_2 patterns is well preserved. Fig. 4*D* shows the OM images of MoS_2 spiral patterns grown from four "growth–detach" cycles on the same SiO_2/Si substrate after water delamination. It was found that the shape of the MoS_2 spiral in each cycle was well reserved and that the reflectance contrast was

uniform under the same illumination. The OM images of SiO_2/Si substrates before growth and after delamination (*SI Appendix*, Fig. S17) show that premade patterns on SiO_2/Si substrate are retained after this simple and clean transfer without visible damage and contamination. From our calculation, the O_2 plasma-treated substrates have lower binding energy with hydrocarbon species (the common contaminate in air) (*SI Appendix*, Fig. S18), which suggests a "contamination-resilient" feature of O-rich surfaces. This could be verified by our observation that the patterned substrates kept for several weeks are still as effective to patterned growth as freshly made. To evaluate the quality of the MoS_2 patterns grown by the recycled growth, we extracted strain (*SI Appendix*, Fig. S19) and carrier concentration maps (Fig. 4*E*) from the spatially resolved Raman analysis (34, 35) on the MoS_2 spirals grown each time using the same SiO_2/Si template. The strain and carrier concentration maps show a relatively small variation, indicating good consistency in the quality of MoS_2 patterns for different cycles. Moreover, the PL spectrum on monolayer MoS_2 from each cycle has few changes on the emission energy and FWHM (*SI Appendix*, Fig. S20). The photoluminescence position mappings (Fig. 4*F*) extracted from the PL spectrum analysis also demonstrate the preserved qualities. After delamination, these MoS_2 patterns floating on a water surface can be easily picked up onto arbitrary substrates, such as transparent quartz (*SI Appendix*, Fig. S21*A*) and flexible mica (*SI Appendix*, Fig. S21*B*), allowing for more efficient integration of complicated 2D device structures.

The key for repeated utilization of the same mask relies on the successful delamination (hence, on the quality of the monolayer MoS_2 patterns). If MoS_2 particles are grown, the patterns are difficult to delaminate by water, which will damage the surface integrity and reduce the lifetime of the master template. With well-controlled growth, successful transfer, and posttreated cleaning, it is anticipated that these prepatterned templates can be used many times. This additive manufacturing method paves the way for broad applications of 2D TMD nanostructures in modern electronics and optoelectronics with much simpler fabrication, lower cost, and higher efficiency.

Methods

To obtain patterned substrates for MoS_2 growth, photolithography and O_2 plasma treatment steps were first carried out as explained above. After removing the photoresist on the patterned SiO_2/Si wafer, the substrate was preannealed at 350 °C for 2 h with 300 standard cubic centimeters per minute (sccm) Ar and 100 sccm H_2 gases. Then, a piece of the patterned substrate was suspended between two SiO_2/Si substrates with predeposited PTAS (via solution dropping). All of these substrates were placed face down on a crucible containing MoO_3 precursor in a 1-inch quartz tube. This crucible was placed in the middle of the heating zone with another smaller tube containing the sulfur crucible upstream close to the cold end of the quartz tube. Before heating, the whole CVD system was purged with 1,000 sccm Ar (99.999% purity) for 3 min. Then, 20 sccm Ar was introduced into the system as a carrier gas. The growth system was heated to 625 °C for 15 min. At around 13 min, the sulfur crucible was pushed into the system by a magnet (as shown in Fig. 3*A*) at a distance of ∼1.5 cm from the left edge of the furnace. The MoS_2 growth was carried out around 620 °C to 630 °C for 3 min under atmospheric pressure. The growth system was finally cooled down to room temperature quickly by opening the furnace and cooling using a fan.

ACKNOWLEDGMENTS. We acknowledge support from Air Force Office of Scientific Research Multidisciplinary University Research Initiative-Foldable and Adaptive Two-Dimensional Electronics Program Grant FA9550-15-1-0514, the Center for Energy Efficient Electronics Science through NSF Grant 0939514, the US Army Research Office through Massachusetts Institute of Technology Institute for Soldier Nanotechnologies Grant 023574, the Center for Integrated Quantum Materials, Science and Technology Center through NSF Grant DMR-1231319 (to Q.J. and Y.L.), and King Abdullah University of Science and Technology Contract OSR-2015-CRG4-2634. Y.H. and D.A.M. acknowledge the Cornell Center for Materials Research for funding through NSF Materials Research Science and Engineering Centers Program DMR-17198751. X.L. acknowledges the support of Boston University.

1. Radisavljevic B, Kis A (2013) Mobility engineering and a metal-insulator transition in monolayer MoS_2. *Nat Mater* 12:815–820.
2. Bertolazzi S, Brivio J, Kis A (2011) Stretching and breaking of ultrathin MoS_2. *ACS Nano* 5:9703–9709.
3. Mak KF, McGill KL, Park J, McEuen PL (2014) Valleytronics. The valley hall effect in MoS_2 transistors. *Science* 344:1489–1492.
4. Wu W, et al. (2014) Piezoelectricity of single-atomic-layer MoS_2 for energy conversion and piezotronics. *Nature* 514:470–474.
5. Feng Q, et al. (2014) Semiconductors: Growth of large-area 2D $MoS_2(1-x)Se_{2x}$ semiconductor alloys (Adv. Mater. 17/2014). *Adv Mater* 26:2763.
6. Radisavljevic B, Radenovic A, Brivio J, Giacometti V, Kis A (2011) Single-layer MoS_2 transistors. *Nat Nanotechnol* 6:147–150.
7. Wang QH, Kalantar-Zadeh K, Kis A, Coleman JN, Strano MS (2012) Electronics and optoelectronics of two-dimensional transition metal dichalcogenides. *Nat Nanotechnol* 7:699–712.
8. Zheng W, et al. (2015) Patterning two-dimensional chalcogenide crystals of Bi_2Se_3 and In_2Se_3 and efficient photodetectors. *Nat Commun* 6:6972.
9. Yu Q, et al. (2011) Control and characterization of individual grains and grain boundaries in graphene grown by chemical vapour deposition. *Nat Mater* 10:443–449.
10. Zhou H, et al. (2013) Thickness-dependent patterning of MoS_2 sheets with well-oriented triangular pits by heating in air. *Nano Res* 6:703–711.
11. Mahjouri-Samani M, et al. (2015) Patterned arrays of lateral heterojunctions within monolayer two-dimensional semiconductors. *Nat Commun* 6:7749.
12. Xue Y, et al. (2016) Scalable production of a few-layer MoS_2/WS_2 vertical heterojunction array and its application for photodetectors. *ACS Nano* 10:573–580.
13. Park W, et al. (2014) Photoelectron spectroscopic imaging and device applications of large-area patternable single-layer MoS_2 synthesized by chemical vapor deposition. *ACS Nano* 8:4961–4968.
14. Cao L, et al. (2013) Direct laser-patterned micro-supercapacitors from paintable MoS_2 films. *Small* 9:2905–2910.
15. Kelly AG, et al. (2017) All-printed thin-film transistors from networks of liquid-exfoliated nanosheets. *Science* 356:69–73.
16. Han GH, et al. (2015) Seeded growth of highly crystalline molybdenum disulphide monolayers at controlled locations. *Nat Commun* 6:6128.
17. Song I, et al. (2014) Patternable large-scale molybdenium disulfide atomic layers grown by gold-assisted chemical vapor deposition. *Angew Chem Int Ed Engl* 53:1266–1269.
18. Kim H-J, Kim H, Yang S, Kwon J-Y (2017) Grains in selectively grown MoS thin films. *Small* 13:1702256.
19. Chen X, et al. (2016) Lithography-free plasma-induced patterned growth of MoS_2 and its heterojunction with graphene. *Nanoscale* 8:15181–15188.
20. Shyu TC, et al. (2015) A kirigami approach to engineering elasticity in nanocomposites through patterned defects. *Nat Mater* 14:785–789.
21. Lamoureux A, Lee K, Shlian M, Forrest SR, Shtein M (2015) Dynamic kirigami structures for integrated solar tracking. *Nat Commun* 6:8092.
22. Blees MK, et al. (2015) Graphene kirigami. *Nature* 524:204–207.
23. Ling X, et al. (2014) Role of the seeding promoter in MoS_2 growth by chemical vapor deposition. *Nano Lett* 14:464–472.
24. Ling X, et al. (2016) Parallel stitching of 2D materials. *Adv Mater* 28:2322–2329.
25. van der Zande AM, et al. (2013) Grains and grain boundaries in highly crystalline monolayer molybdenum disulphide. *Nat Mater* 12:554–561.
26. Kang K, et al. (2015) High-mobility three-atom-thick semiconducting films with wafer-scale homogeneity. *Nature* 520:656–660.
27. English CD, Shine G, Dorgan VE, Saraswat KC, Pop E (2016) Improved contacts to MoS_2 transistors by ultra-high vacuum metal deposition. *Nano Lett* 16:3824–3830.
28. ten Wolde PR, Frenkel D (1997) Enhancement of protein crystal nucleation by critical density fluctuations. *Science* 277:1975–1978.
29. Burns RP, DeMaria G, Drowart J, Grimley RT (1960) Mass spectrometric investigation of the sublimation of molybdenum dioxide. *J Chem Phys* 32:1363–1366.
30. Kumari L, et al. (2007) X-ray diffraction and Raman scattering studies on large-area array and nanobranched structure of 1D MoO_2 nanorods. *Nanotechnology* 18:115717.
31. Li H, Li Y, Aljarb A, Shi Y, Li L-J (2018) Epitaxial growth of two-dimensional layered transition-metal dichalcogenides: Growth mechanism, controllability, and scalability. *Chem Rev* 118:6134–6150.
32. Chhowalla M, et al. (2013) The chemistry of two-dimensional layered transition metal dichalcogenide nanosheets. *Nat Chem* 5:263–275.
33. Wang X, Feng H, Wu Y, Jiao L (2013) Controlled synthesis of highly crystalline MoS_2 flakes by chemical vapor deposition. *J Am Chem Soc* 135:5304–5307.
34. Michail A, Delikoukos N, Parthenios J, Galiotis C, Papagelis K (2016) Optical detection of strain and doping inhomogeneities in single layer MoS_2. *Appl Phys Lett* 108:173102.
35. Chae WH, Cain JD, Hanson ED, Murthy AA, Dravid VP (2017) Substrate-induced strain and charge doping in CVD-grown monolayer MoS_2. *Appl Phys Lett* 111:143106.